ELSEVIER

Contents lists available at ScienceDirect

### North American Spine Society Journal (NASSJ)

journal homepage: www.elsevier.com/locate/xnsj



#### **Basic Science**

# Towards a validated patient-specific computational modeling framework to identify failure regions in traditional growing rods in patients with early onset scoliosis



Aakash Agarwal<sup>a,\*</sup>, Manoj Kodigudla<sup>a</sup>, Amey Kelkar<sup>a</sup>, Daksh Jayaswal<sup>a</sup>, Vijay Goel<sup>a</sup>, Vivek Palepu<sup>b</sup>

- <sup>a</sup> Engineering Center for Orthopaedic Research Excellence (E-CORE), Department of Bioengineering and Orthopaedic Surgery, University of Toledo, 2801 West Bancroft Street. Toledo. OH 43606 USA
- <sup>b</sup> Center for Devices and Radiological Health, Office of Science and Engineering Laboratories, Division of Applied Mechanics, U.S. Food and Drug Administration, Silver Spring, MD 20993 USA

#### ARTICLE INFO

# Keywords: Biomechanics Growing rods Early onset scoliosis Finite element analysis Patient specific modelling Rod failures

#### ABSTRACT

*Background:* While growing rods are an important contribution to early-onset scoliosis treatment, rod fractures are a common complication that require reoperations. A recent retrieval analysis study performed on failed traditional growing rods revealed that there are commonalities among patient characteristics based on the location of rod fracture. However, it remains unknown if these locations correspond to high stress regions in the implanted construct

Methods: A patient-specific finite element scoliotic model was developed to match the pre-operative (pre-op) scoliotic curve of a patient as described in previously published articles, and by using the patient registry information along with biplanar radiographs. A dual stainless-steel traditional growing rod construct was implanted into this scoliotic model and the surgical procedure was simulated to match the post-operative (post-op) scoliotic curve parameters. Muscle stabilization and gravity was simulated through follower load application. Rod distraction magnitudes were chosen based on pre-op to post-op cobb angle correction, and flexion bending load was simulated to identify the high stress regions on the rods.

Results: The patient-specific finite element model identified two high stress regions on the posterior surface of the rods, one at mid construct and the other adjacent to the distal anchors. This correlated well with the data obtained from the retrieval analysis performed by researchers at U.S. Food and Drug Administration (FDA) which showed the posterior surface of the rod as the fracture initiation site, and the three locations of failure as mid-construct, adjacent to distal anchors, and adjacent to tandem connector.

Conclusions: The result of this study confirms that the high stress regions on the growing rods, as identified by the FEA, match the fracture prone sites identified in the retrieval analysis performed at the FDA. This proof-of-concept patient-specific approach can be used to predict sites prone to fracture in growing rods.

#### **Background**

Early-onset scoliosis is an understudied field of scoliosis as compared to the adolescent and adult counterparts. This is in part due to the concurrent growth and development happening in these young patients, which makes the surgical correction a long-term commitment for both patients and surgeons. Halting the deformity alongside sustaining growth is challenging for the innovators in the field. Thus, few commercially available therapeutic device options (e.g., traditional growing rods, magnetically controlled growing rods, and growth guidance

system) are available [1-8]. Although the treatment philosophies are different among these technologies, the common complication of rod fracture remains. Several clinical studies reported rod fractures in traditional and magnetic growing rod constructs with high occurrence rates (greater than 25%) [9-16].

A recent study performed by the U.S. Food and Drug Administration (FDA) on retrieved failed traditional growing rods from thirty-six patients revealed that the traditional growing rods fractured at a few common locations. The authors found that the failure locations were: mid-construct, adjacent to the tandem connector, and adjacent to the

E-mail address: aakash.agarwal@utoledo.edu (A. Agarwal).

<sup>\*</sup> Corresponding author.

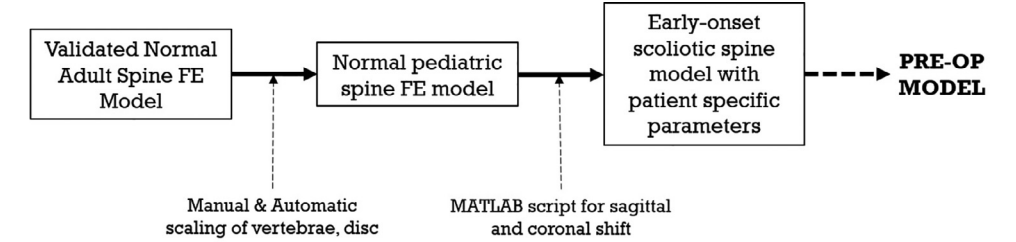


Fig. 1. Overview of methodology used to develop a patient-specific pre-operative (pre-op) finite element model. A validated adult spine model was first scaled down to the anatomical equivalent of a early-onset scoliosis spine, following which a MATLAB script was used to induce coronal and sagittal deformity to match the spine model pre-op parameters with clinical registry data.

distal anchor [17]. However, it remains unknown if these are truly the high stress regions, from a biomechanical perspective, for traditional growing-rods implanted in patients that result in rod fracture.

Finite element analysis (FEA) can be of great benefit in performing biomechanical evaluations to identify potential failure regions on medical devices in comparison to other bench testing options [18-21]. For example, FEA is a computational research method that can overcome inherent problems of cadaver experiments, such as low availability of appropriate donor pool with relevant scoliotic curves, high geometrical and bone quality variability among different specimens, and limitations in the accuracy of stress/strain measurements on implanted constructs.

In the case of addressing the traditional growing rod failures, FEA can simulate the effects of a variety of physiological scenarios (e.g., different Cobb angles) on an implant and predict biomechanical parameters such as stresses/strains throughout that implant. This kind of analysis is challenging, if not impossible, in a physical experiment and such data can be paramount in analyzing failure modes of an implant [22].

Recently, patient-specific FEA was used in the field of orthopedics to identify high stress regions of implants or adjoining anatomical structures under different loading regimes and investigate the underlying cause [23,24]. A patient-specific approach in FEA usually involves the three-dimensional reconstruction of the anatomy of an individual patient based on CT/MRI images or other individual clinical parameters such as implant type and dimensions. Following this, the patient-specific or individualized FEA model can be used to simulate different clinical scenarios. Such models may provide a diagnosis for a particular set of symptoms, a prognosis of a particular ailment, or predict the outcome of a clinical treatment. Although, patient-specific FEA is typically more labor intensive and time consuming, it accounts for patient characteristics which may make results more meaningful when compared to a more generalized approach [25].

This patient specific FEA approach has been used previously in fields such as orthodontics, lower limb prosthetics, and fracture fixation techniques to identify potential regions of implant failure [26–32]. In the field of early onset scoliosis, the patient-specific approach was used to analyze the forces on implants following different correction maneuvers and different instrumentation strategies [33–35].

Building upon prior successes, the objective of the current study was to use a patient-specific approach with FEA and identify the high stress regions on traditional growing rods in patients with early-onset scoliosis. Furthermore, we established a methodology towards validation of the patient-specific approach. We aimed to apply patient-specific parameters to an FEA spine model, determine the high stress regions on the rods, and then compare those high stress regions with rod failure locations reported by a clinical implant retrieval study.

#### Methods

Finite element analysis

#### Pre-operative scoliotic FEA model development

A patient-specific FEA model of the thoracolumbar spine (T1-S1) was developed to match the pre-operative (pre-op) scoliosis curve of a patient (patient no. 4), as described by the authors of previously published work, and by using patient registry (Growing Spine Study Group, San

Diego, CA) information along with biplanar radiographs, Fig. 1 [36-40]. In brief, a normal pediatric spine model was used as the template to produce the patient-specific early-onset scoliotic model (Age = 10.8 years) [41,42].

A MATLAB script (MATLAB Inc, Natick, MA) was used to create patient-specific coronal and sagittal deformity in the base template (normal) pediatric spine model [43]. The boundary conditions for the coronal and sagittal deformity (Cobb Angle, Thoracic Kyphosis, Lumbar Lordosis, and the thoracolumbar spine (T1-S1) height) were obtained from the patient's pre-op biplanar radiographs. An image processing software (Surgimap, Nemaris Inc., New York, NY) was used to quantify the deformity characterizing parameters and boundary conditions from the patient radiographs, Fig. 2. The user variability analysis on taking the patient radiographic measurements using Surgimap software shall be analyzed as a part of a future study. The final pre-op scoliotic curve parameters for the spinal model were within  $\pm$  5 degrees of the radiographic measurements [44,45].

The patient-specific data regarding material, geometry, and type of implants was obtained from the clinical patient registry. Dual stainless-steel traditional growing rod constructs with tandem connectors were created for implantation into the scoliotic model using pedicle screws as bone anchors. Rods were designed to match the coronal and sagittal profile obtained from the post-operative (post-op) patient radiographs.

The levels of pedicle screw implantation were also obtained from the post-op radiographs. The implants simulated include rods of 4.5 mm diameter, screws of 3.5 mm diameter in the thoracic region and 4.5 mm diameter in the lumbar region, and tandem connectors of 70 mm length. The screws were simulated from T2-T4 and L1-L3, connected using rods and tandem connectors. The material properties, the constitutive laws, and the types of elements used for the entire model are described in Table 1.

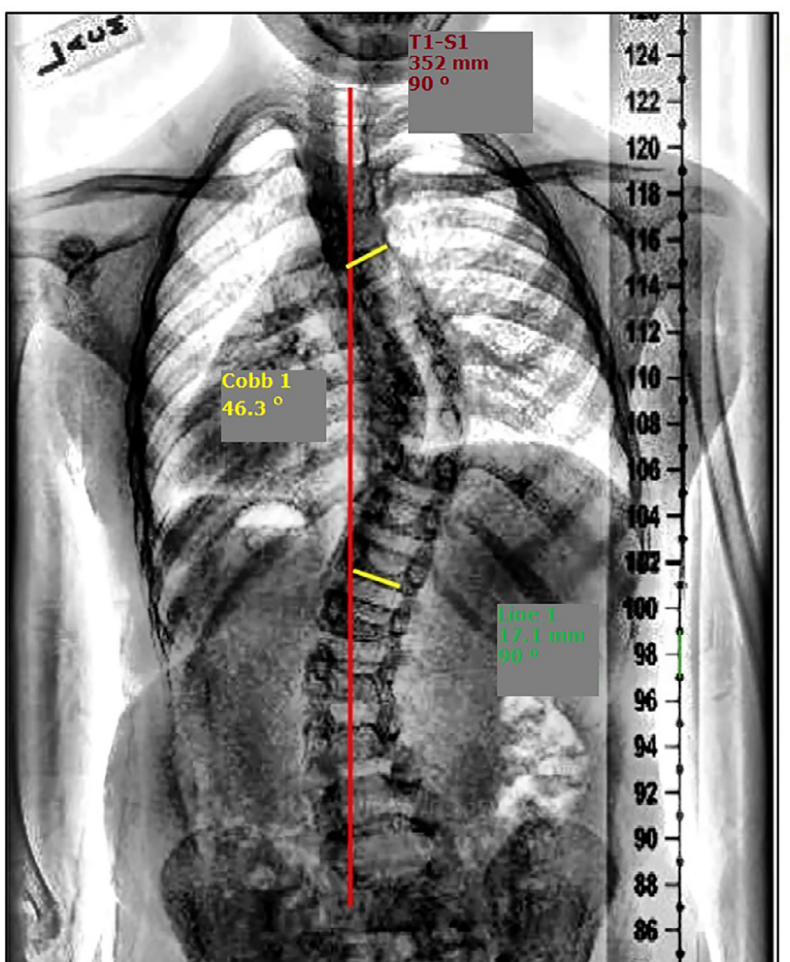
Abaqus solver version 6.14 (Dassault Systems, Johnston, RI) was used for the analysis. The default direct, full newton solver was used in this study. No custom sub-routines, convergence criteria, solution strategies, solution modules or material models were created in the Abaqus solver for this study. Only off the shelf and default material models, modules, and sub-routines from the Abaqus solver were used. Therefore, a code verification study for the finite element solver was deemed unnecessary.

Mesh convergence study of spinal rods

A mesh convergence study was undertaken to determine the optimal mesh for the rod. A model of the spinal rod was used for this study and it was meshed with element sizes ranging from 0.2 to 5 mm, **Appendix 1a**. A simple cantilever bending test was simulated with one end of the rod fixed in all directions and 100 N of compressive load was applied to the other end of the rod to create a bending moment. This loading was simulated to create the effect of flexion bending moment on the rod. The time taken to complete the analysis by the Abaqus solver and the stresses on the rod were plotted for each element size.

The results of the mesh converge study demonstrated that as the number of elements in the mesh increased 14 folds, the bending stress value increased by 4%. An element size that resulted in a bending stress value of less than 5% when compared to the next incremental element size, was selected as an optimal element size. Therefore, an element size

Left



Right

**Fig. 2.** Example of methodology used to quantify deformity parameters from patient radiographs using Surgimap image processing software. Measurements were taken preoperatively and post-operatively in both coronal as well as sagittal planes and were matched to the FEA model.

**Table 1** Element type and material properties used for the FEA model components [35-39,42].

Model component	Element type	Constitutive law	Elastic Modulus (MPa) / Poisson's Ratio	
Cortical Bone	Isotropic Linear Elastic Hexahedral Elements (C3D8)	Hooke's law	75/0.29	
Cancellous Bone	Isotropic Linear Elastic Hexahedral Elements (C3D8)	Hooke's law	75/0.29	
Growth Plate	Isotropic Linear Elastic Hexahedral Elements (C3D8)	Hooke's law	25 / 0.4	
Posterior Boney Elements	Isotropic Linear Elastic Hexahedral Elements (C3D8)	Hooke's law	200 / 0.25	
Nucleus Pulposus	Isotropic Linear Elastic Hexahedral Elements (C3D8H)	Hooke's law	1 / 0.499	
Annulus (Ground)	Hyper-elastic Hexahedral Elements (C3D8)	Neo-Hookean	C10 = 0.348, $D1 = 0.3$	
Annulus (Fibers)	Rebar Elements (REBAR)	n/a	357-550	
Facet Joints	Nonlinear Soft Contact Gap Elements (GAPUNI)	Pressure-overclosure relationship	12000	
Ligaments	Tension Only, Hypo-elastic Truss Elements (T3D2)	•	90% of Adult Ligament Values	
Pedicle Screws	Isotropic Linear Elastic Hexahedral Elements (C3D8)	Hooke's law	193000 / 0.29	
Rods	Isotropic Linear Elastic Hexahedral Elements (C3D8)	Hooke's law	193000 / 0.29	
Tandem Connector	Isotropic Elastic Hexahedral Elements (C3D8)	Hooke's law	193000 / 0.29	

of 0.5 mm was chosen to be optimal for this study. A stress distribution and computational time comparison was also performed on different rod geometries for the simple bending experiment, **Appendix 1b**.

#### Post-operative scoliotic FE model development

The developed pre-op patient-specific scoliotic model was modified to simulate the surgical procedure and thus match the post-op scoliotic curve parameters, Fig. 3. First, correction of the sagittal curvature was achieved by applying a flexion of  $5^{\circ}$  to T1 vertebra and a flexion of  $10^{\circ}$  to L4 vertebra of the un-instrumented scoliotic spine model.

The exact degree of thoracic flexion and the lumbar extension applied to the spine FEA model above was obtained using an iterative process until the necessary post-op correction was achieved. This correction was done to both match the sagittal profile of rods obtained from

post-op biplanar radiographs of the patient, and to obtain the stresses generated on the rod (simulation of rod attachment), Fig. 4. The final post-op scoliotic curve parameters for the spinal model were within  $\pm$  5° of the radiographic measurements [44,45].

#### Contact and loading conditions

The spinal instrumentation was implanted into the sagitally corrected spinal model. A rigid tie constraint was defined between the pedicle screw-bone interface and the spinal rod-pedicle screw interface. The distal (bottom) rods on either side were also rigidly tied to the respective tandem connectors. A surface to surface interaction with low friction and "hard contact" type was defined between the proximal (top) rods and the tandem connectors. The coefficient of friction was kept as low as allowed (coefficient = 0.1) by the solver to simulate smooth slid-

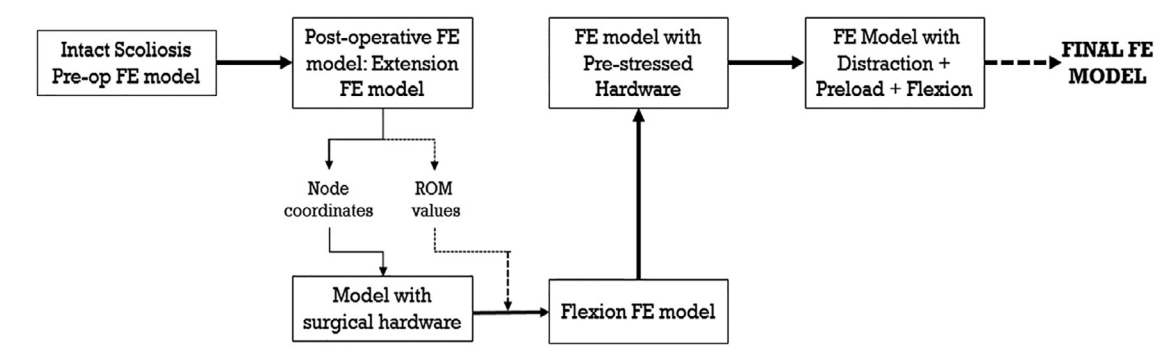
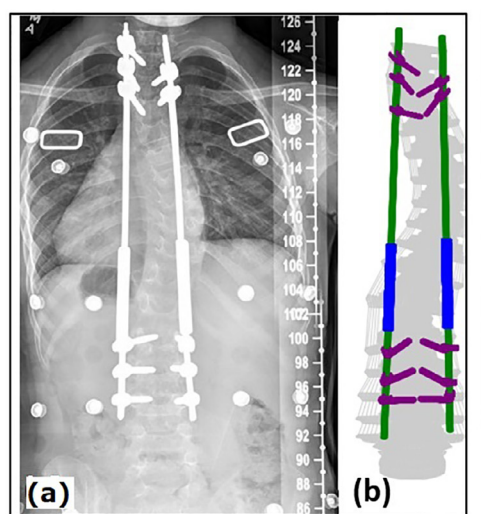
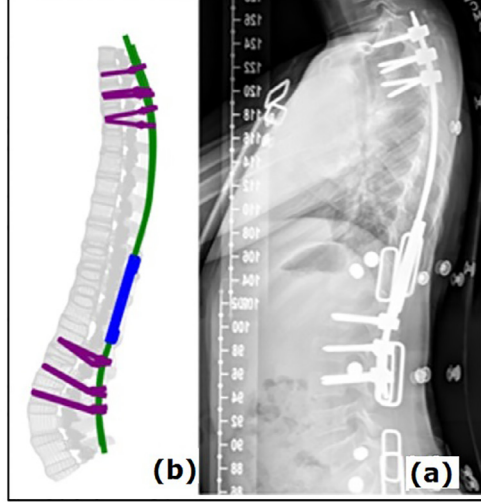


Fig. 3. Overview of FEA methodology used to simulate a post-operative (post-op) patient-specific finite element model. The pre-operative scoliotic model was loaded iteratively in flexion/extension loading to achieve necessary sagittal post-op correction and to capture stresses generated on the rods. Finally, distraction, preload, and flexion loads were sequentially applied to simulate growing rod technique and evaluate rod stresses.





**Fig. 4.** Comparison of the patient specific finite element model with the patient radiographs. (a) The radiographic image and (b) patient specific finite element model counterparts are shown for coronal (Left) and sagittal profiles (Right) respectively.

**Post-Op Coronal View** 

## **Post-Op Sagittal View**

ing between the rods and the tandem connector. Hard contact type was defined to limit the surface penetrations during the scoliosis correction procedure. No contact controls were used in this analysis which was the default setting in Abaqus v6.14.

The surgical stresses exerted on the instrumentation from rod attachment were calculated as described earlier and were accounted for in the initial step of the analysis. Next, 7 mm of bilateral longitudinal distraction was applied to the spine model to correct the deformity in the coronal plane and then a follower load was applied to account for muscle stabilization and segmental gravity. The exact degree of bilateral distraction applied to the spine model was obtained using an iterative process until the necessary post-op surgical correction was achieved.

The follower load technique simulated the load at different vertebral levels due to upper body mass and muscle contractions as described by Schultz et al. [46]. The loads were applied from the T1 to S1 levels as a percentage of the patient's body weight (38.5 kg), Table 2. A flexion moment of 1Nm was applied to simulate forward bending which is a common bending activity related with rod failures in children as identified from fracture initiation sites on the retrieved rods [17]. A flexion moment of 0.52 Nm was identified via inverse dynamics approach to result in a range of motion similar to an adult spine (at 7.5 Nm). Thus, a bending moment of 1 Nm was chosen to simulate a worst-case bending scenario based on this data. The inferior endplate (base) of the S1 vertebra was fixed in all directions in all these steps.

**Table 2**Follower load applied based on percentage of body weight from T1 to L5 [45].

Level	Percentage of Body Weight (%)	Weight Applied (kg)	Load (N)
T1	14	5.4	52.9
T2	16.7	6.4	63.1
T3	19.4	7.5	73.3
T4	22.1	8.5	83.5
T5	24.8	9.5	93.7
T6	27.5	10.6	103.9
T7	30.1	11.6	113.7
T8	32.8	12.6	123.9
T9	35.5	13.7	134.1
T10	38.2	14.7	144.3
T11	40.9	15.7	154.5
T12	43.6	16.8	164.7
L1	46.3	17.8	174.9
L2	49.0	18.9	185.1
L3	51.7	19.9	195.3
L4	54.4	20.9	105.5
L5	57.0	21.9	215.3

#### Data analysis

Spatial distribution of stresses was recorded on the rods, after (1) surgical correction, application of distraction forces and follower loads, and (2) at the end of 1 Nm of flexion bending. The rod regions were di-

**Table 3**Comparison of patient characteristics and demographics at pre-operative time point between previously published failed rod retrieval patient group and the single patient (patient no. 4) used for FEA in this study [17].

Patient parameters	Failed rod retrievals $n=14$ Patients Mean $\pm$ SD (range)	Patient no. 4 data used for computational model
Gender	6 females (43%)	Male
Age (years)	$8.1 \pm 2.6(2.7-10.7)$	10.8
Weight (kg)	$22.4 \pm 7.0(11.1-38.5)$	38.5
Cobb Angle (Degrees)	$77 \pm 14^{\circ}(48 \text{ to } 96^{\circ})$	48°
Kyphosis (Degrees)	$37 \pm 31^{\circ}(-25 \text{ to } 87^{\circ})$	26°
Lordosis (Degrees)	$-58 \pm 25^{\circ}(-87 \text{ to } 6^{\circ})$	-45°

vided into types of surfaces, (i.e. interacting surfaces and non-interacting surfaces), and locations (i.e. proximal, mid-construct, and distal). Interacting surfaces refers to all the surfaces where two or more bodies are in permanent contact whereas non-interacting surfaces are the free surfaces.

#### Qualitative validation

#### Retrieval study

Results published in the prior retrieval study were used as a basis where characteristics and demographics were analyzed from patients with failed traditional growing rod constructs (n=18 constructs from 14 patients) [17]. Failure analyses were reported in this prior study on the fractured surfaces to identify failure mechanisms as well as areas of damage and corrosion. Published results indicated that these failed rods were fractured due to bending fatigue under flexion motion. Moreover, patient characteristics and construct configuration dictated failure at three distinct locations along the construct: (1) mid-construct, (2) adjacent to the tandem connector, or (3) adjacent to the distal anchor foundation.

#### Computational modeling and simulation

For computational model validation, four of fourteen patients from the failed rod retrieval study were selected based on the quality of information from the registry data and radiographs essential for modeling [17]. The goal of this project is to develop a patient specific FEA model for each of these four patients (patient numbers 1, 2, 3, & 4 respectively) and validate the high stress regions on the traditional growing rod constructs with corresponding failure location information.

Although one (patient no. 4) of these four selected patients did not have any rod fracture location data, the scoliotic curve of this patient had a lower cobb angle facilitating relative ease in modeling compared to the other three patients. Therefore, as a proof of concept, we selected this patient (patient no. 4, characteristics and demographics presented in Table 3) for modeling in this study which allowed for verification of the modeling framework adopted for the patient-specific scoliosis FEA.

As a step towards validation, we aim to investigate the high stress regions induced in the traditional growing rods for this patient under flexion bending and compare the outcomes with the rod failure locations that were determined for the entire pool of retrieval study patients. Once the modeling framework has been verified and validated, the patient specific models for the other patients shall be developed using the process established by the framework.

#### Results

The comparison between pre-op clinical parameters for the finite element model and the Surgimap data from pre-op biplanar radiographs are listed in Table 4. The comparison between post-op clinical parameters for the finite element model and the Surgimap data from the post-op biplanar radiographs are listed in Table 5. The parameters predicted by the patient-specific finite element model matched well within  $\pm 5$  degrees of the radiographic measurements.

**Table 4**Comparison of pre-surgical clinical parameters between the finite element model and data calculated from clinical registry radiographs.

Pre-Surgical Parameter	Finite element model data	Radiographic data	
Cobb angle (degrees)	46	46	
Lordosis (degrees)	45	45	
Kyphosis (degrees)	26	26	
T1-S1 height (mm)	349	352	

**Table 5**Comparison of post-surgical clinical parameters between the finite element model and data calculated from clinical registry radiographs.

Post-Surgical Parameter	Finite element model data	Radiographic data	
Cobb angle (degrees)	37	35	
Lordosis (degrees)	52	52	
Kyphosis (degrees)	28	30	
Change in T1-S1 height (mm)	6.7	7.1	

Figs. 5 & 6 show the spatial distribution of stresses on the distal region. The posterior surface was examined because the fracture initiation sites identified in previous retrieval analyses were on the posterior surface. The high stress region observed on the bottom left rod matched with one of the three (adjacent to distal anchor foundation) clinical fracture locations from the prior retrieval analysis data. Figs. 7 & 8 show the spatial distribution of stresses on the mid-construct region (belonging to top rods for this patient). The high stress regions in this case matched with another clinical fracture location (mid-construct region). Figs. 9 & 10 show the spatial distribution of stresses on the proximal region. The stress distributions, magnitudes, and maximums were similar between models with and without flexion moment loading conditions.

#### Discussion

A retrieval analysis by Hill et al has shown that the posterior surface of the rod is the fracture initiation point with commonalities among patients based on the rod fracture location: mid-construct, adjacent to distal connector, and adjacent to tandem [17]. A detailed biomechanical (kinetic) FEA model can verify if the commonality in fracture regions were indeed biomechanically prone to fracture. Often, these fractures could also be a result of patient-specific variabilities (traumatic and sudden exposure to uncommon physical undertakings, accidents etc.) that are unrelated to the construct's geometry and may not occur under normal circumstances.

In absence of aforementioned variability, the results of our study qualitatively confirmed two fracture locations as the high stress regions (i.e. mid construct & adjacent to distal anchors) for this patient. However, the third fracture site, adjacent to the tandem connector, was not geometrically relevant for this patient's instrumentation layout and will be the subject of an ongoing multi-patient FEA study.

Another interesting result of this study was that the rod stresses did not increase much with the addition of low or high flexion bending magnitudes (0.25 or 1 Nm respectively, Table 6). This result aligns well with the previously published literature which concluded that high stresses

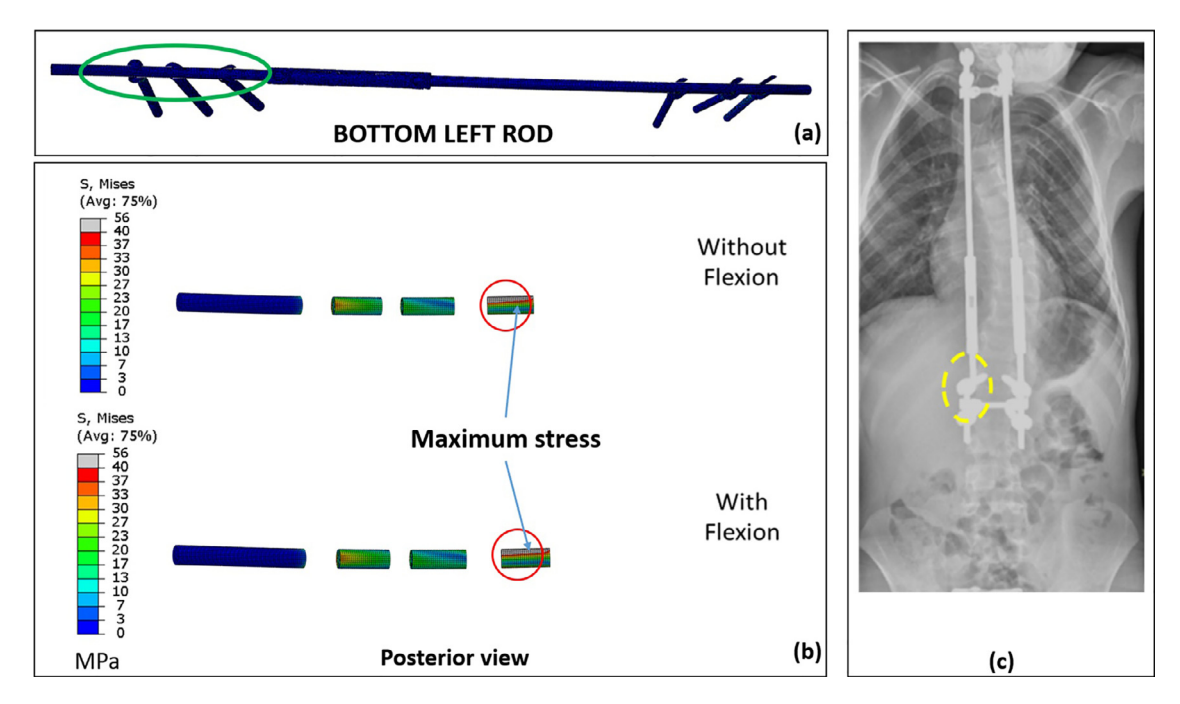


Fig. 5. Stress distribution plot of bottom left rod (convex side) from patient specific traditional growing rod FEA simulation. The maximum stress regions on rod match with one of the three clinical rod failure locations obtained from retrieval analysis data (Hill et al.) (a) FE construct showing bottom left rod with tandem connector and screws that were used as part of the traditional growing rod construct simulated in the patient specific FEA model (the distal region is encircled). (b) Regions with maximum stress on bottom left rod (excluding interacting surfaces), simulated for FEA cases of without and with flexion bending load. (c) An example radiographic image taken from Hill et al. to show clinical rod-failure location (encircled) near distal anchor.

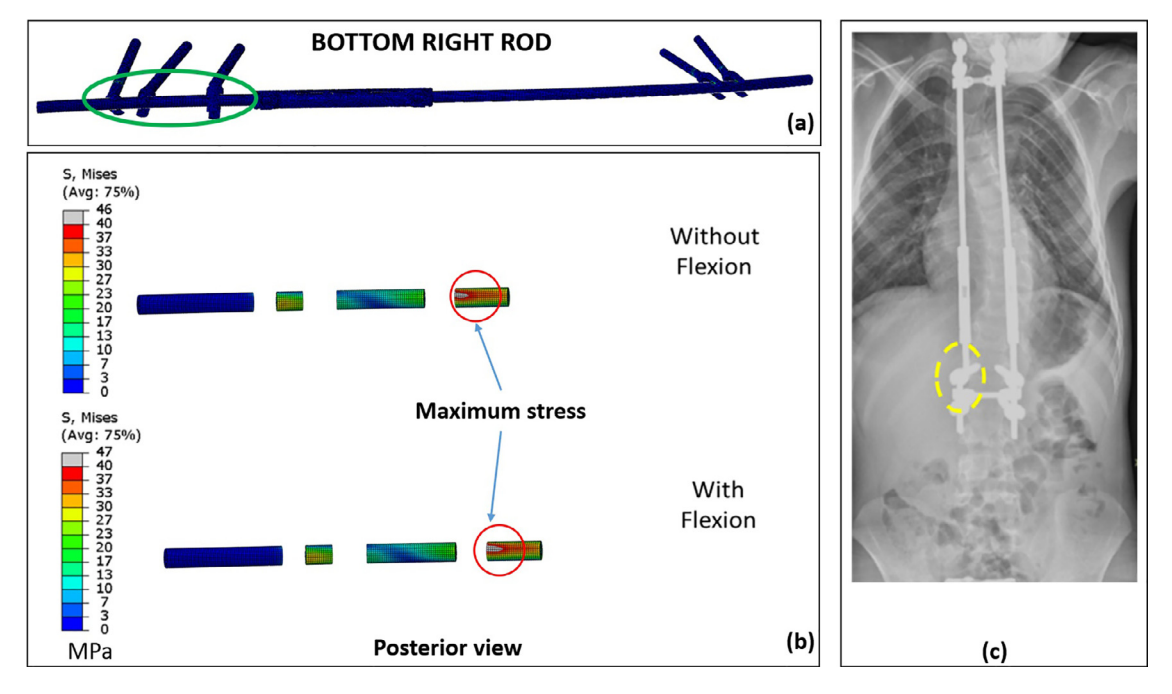


Fig. 6. Stress distribution plot of bottom right rod (concave side) from patient specific traditional growing rod FEA simulation. The maximum stress regions on rod match with one of the three clinical rod failure locations obtained from retrieval analysis data (Hill et al.) (a) FE construct showing the bottom right rod with tandem connector and screws that were used as part of the traditional growing rod construct simulated in the patient specific FEA model (the distal region is encircled). (b) Regions with maximum stress on bottom right rod (excluding interacting surfaces), simulated for FEA cases of without and with flexion bending load. (c) An example radiographic image taken from Hill et al. to show clinical rod-failure location (encircled) near distal anchor.

on the rod could be generated because of factors like patient's weight, and distraction forces [37,38]. In addition, a concave-convex (left and right rods) bias on the stresses was not observed. The overall stress magnitudes on the rods were lower than previously reported values in the literature because the 7 mm distraction in this patient-specific model

only resulted in a reaction force magnitude of 39 N (increases to 81 N after follower load application) [38,39].

Moreover, recent reports suggest that distraction forces generated in patients after dual growing rod surgery is at least 100 N [47]. Thus, the magnitude of stresses reported in this study seem to be on the lower

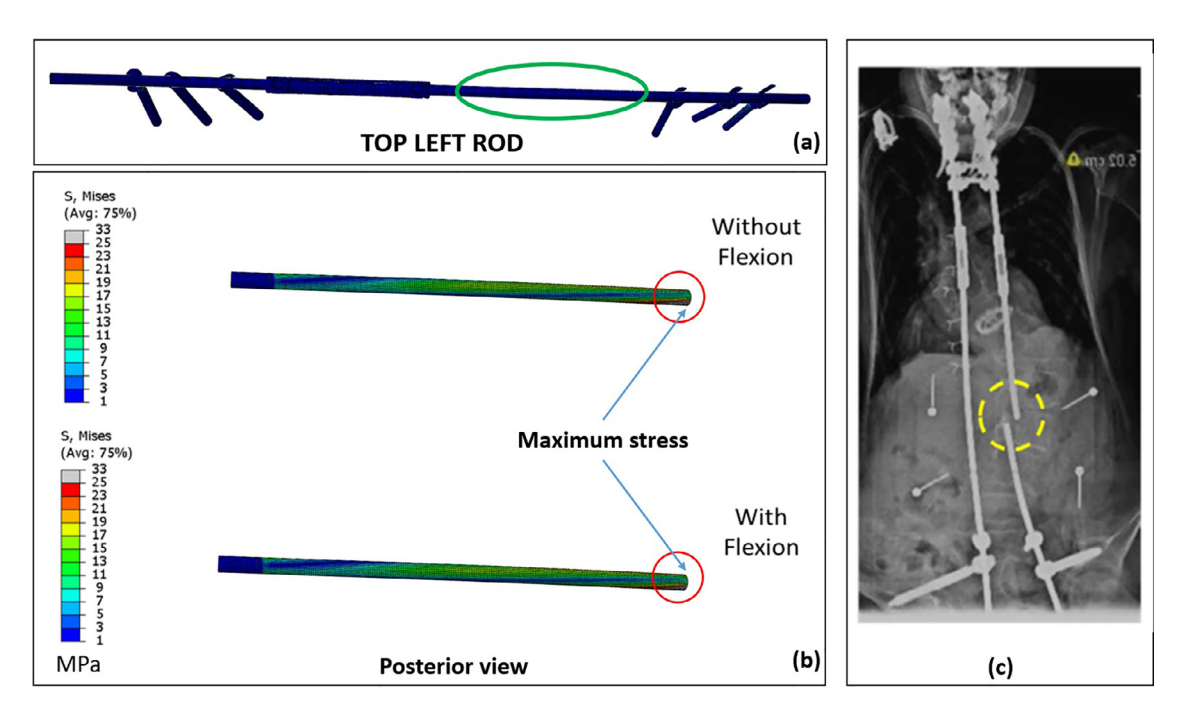


Fig. 7. Stress distribution plot of top left rod (convex side) from patient specific traditional growing rod FEA simulation. The maximum stress regions on rod match with one of the three clinical rod failure locations obtained from retrieval analysis data (Hill et al.) (a) FE construct showing the top left rod with tandem connector and screws that were used as part of the traditional growing rod construct simulated in the patient specific FEA model (the mid-construct region is encircled). (b) Regions with maximum stress on top left rod (excluding interacting surfaces), simulated for FEA cases without and with flexion bending motion. (c) An example radiographic image taken from Hill et al. to show clinical rod-failure location (encircled) near mid-construct. Note: Maximum stress on the top left rod lies near the proximal end (49MPa, documented in Table 6), this figure shows local maximum stress.

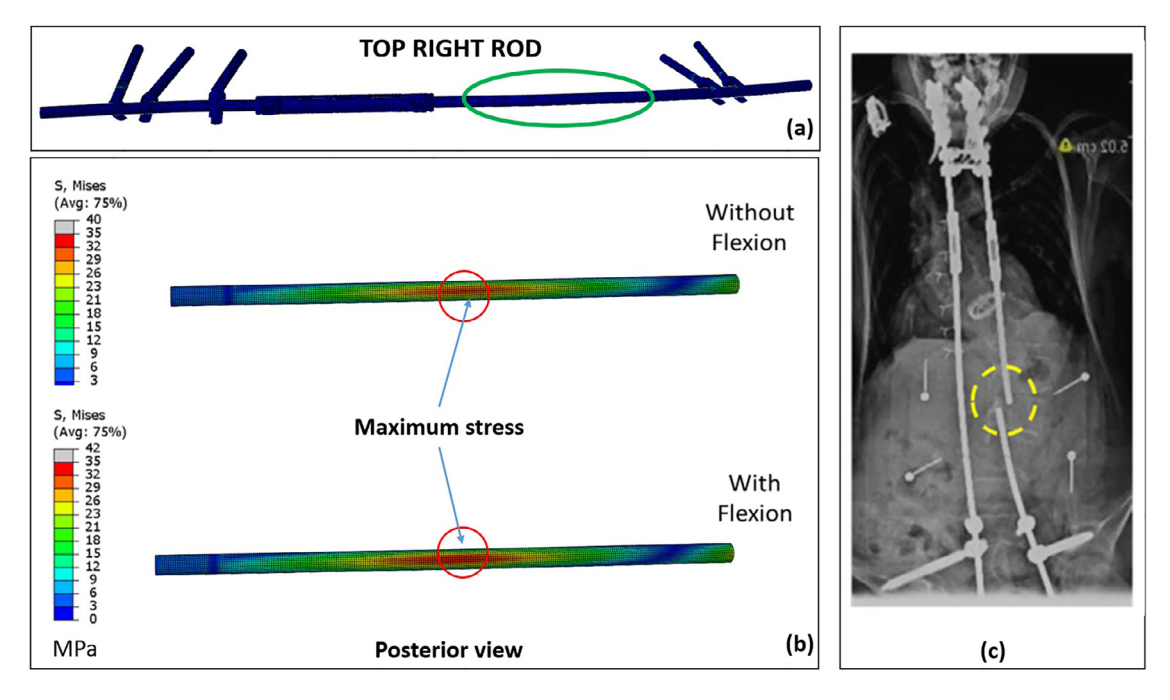


Fig. 8. Stress distribution plot of top right rod (concave side) from patient specific traditional growing rod FEA simulation. The maximum stress regions on rod match with one of the three clinical rod failure locations obtained from retrieval analysis data (Hill et al.) (a) FE construct showing the top right rod with tandem connector and screws that were used as part of the traditional growing rod construct simulated in the patient specific FEA model (the mid-construct region is encircled). (b) Regions with maximum stress on top right rod (excluding interacting surfaces), simulated for FEA cases of without and with flexion bending load. (c) An example radiographic image taken from Hill et al. to show clinical rod-failure location (encircled) near mid-construct. Note: Maximum stress on the top right rod lies near the proximal end (51MPa, documented in Table 6) and this figure shows local maximum stress.

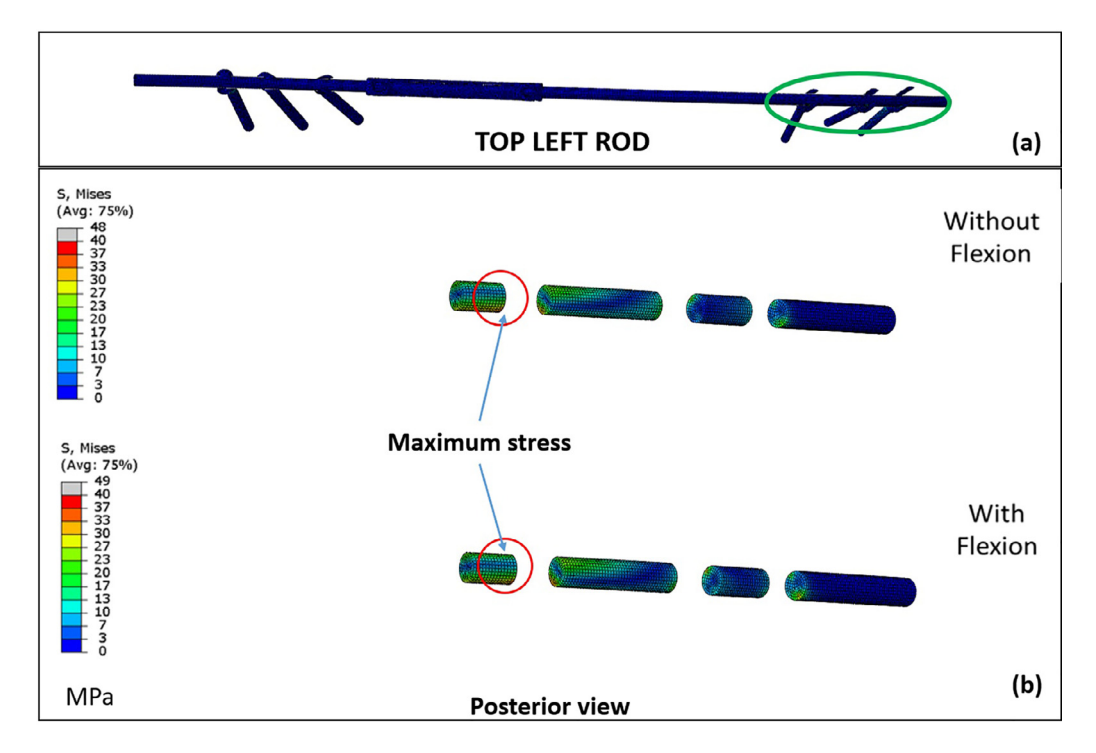


Fig. 9. Stress distribution plot of top left rod (convex side) from patient specific traditional growing rod FEA simulation. (a) FE construct showing the top left rod with tandem connector and screws that were used as part of the traditional growing rod construct simulated in the patient specific FEA model (proximal region is encircled). (b) Regions with maximum stress on top left rod (excluding interacting surfaces), simulated for FEA cases of without and with flexion bending load.

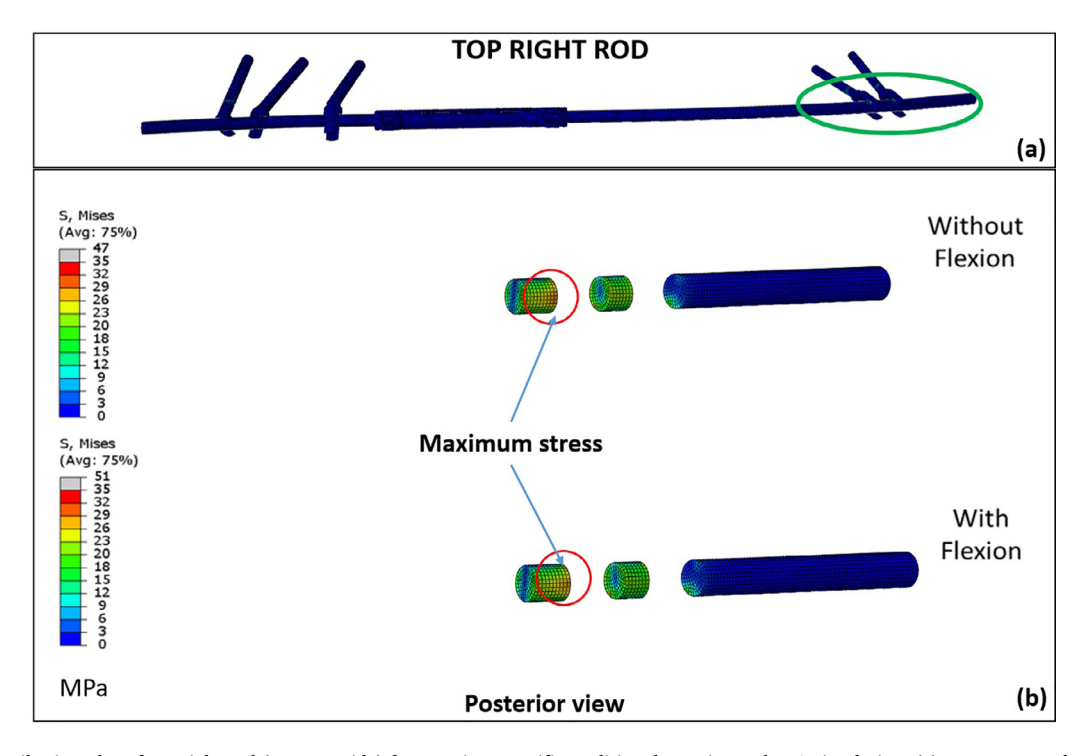


Fig. 10. Stress distribution plot of top right rod (concave side) from patient specific traditional growing rod FEA simulation. (a) FE construct showing the top right rod with tandem connector and screws that were used as part of the traditional growing rod construct simulated in a patient specific FEA model (the proximal region is encircled). (b) Regions with maximum stress on top right rod (excluding interacting surfaces), simulated for FEA cases without and with flexion bending load.

spectrum, and therefore, these numerical values should not be used as a metric for estimating the rod stress magnitude. Readers are advised to focus on the trend and spatial distribution of stress plots more than the actual magnitude, as these stresses would vary among patients and may even increase with consecutive distractions for each individual (due to changes in spinal flexibility and/or autofusion) [46].

The patient-specific FEA approach has great potential to identify high risk regions on medical devices under different loading regimes and may help in understanding the underlying cause of device failures. For example, Shim et al used patient-specific FEA to identify regions of failure in fixation devices used for treating pelvic ring fractures [26]. Several studies have been published where this modeling approach was

Table 6
Comparison of stresses (MPa) observed on the rods after varying the degree of flex-

St	ress Comparison Step 2 (Follower Load)	step 3 (Flo 0.25 Nm		0.75 Nm	1.00 Nm
Bottom Rod_left	56 MPa	56 MPa	56 MPa	56 MPa	56 MPa
Bottom Rod_Right	46 MPa	46 MPa	47 MPa	47 MPa	47 MPa
Top Rod_Left	48 MPa	48 MPa	48 MPa	49 MPa	49 MPa
Top Rod_Right	47 MPa	48 MPa	49 MPa	50 MPa	51 MPa

also used to predict device failures in femoral stems and orthodontic implants [27–32].

In the field of early onset scoliosis, Wang et al and Le Naveaux et al used the patient-specific approach to analyze the effect of different correction maneuvers and different instrument strategies on the three-dimensional adolescent idiopathic curve correction as well as the forces at the bone-implant interface. In brief, Wang et al analyzed the effect of rod contouring on the thoracic kyphosis, cobb angle correction, and screw pullout forces [33]. Similarly, Le Naveux et al used patient-specific idiopathic scoliotic models to assess the effect of the implant density/number of screws used on the thoracic kyphosis, cobb angle correction, and screw pullout forces [34]. To our knowledge, the present study is the first in the literature of early onset scoliosis to develop a patient-specific FEA framework with the help of clinical registry information to identify and validate the high stress regions of traditional growing rods against their fracture location data obtained from the retrieval analysis.

The current study has some limitations, one being the comparison of a single patient FEA model outcomes against a pool of retrieval analysis patient data. We believe that a patient-specific retrieval analysis data for each individual model would be ideal. However, the current data are a first step towards performing such simulations in our ongoing multipatient study.

Another limitation is the user uncertainty introduced due to the use of a single operator obtaining the boundary conditions for coronal and sagittal deformity from patient's pre-op and post-op biplanar radiographs using Surgimap software. This uncertainty will be quantified and analyzed in our future work for the ongoing multi-patient study.

Similarly, another uncertainty is introduced to the model due to the use of spine material properties documented in published literature. However, it becomes cumbersome to extract the patient-specific material properties for this kind of study where human subjects are involved. Furthermore, this material property uncertainty may mainly affect the magnitude of spinal range of motion, which may in turn change the amplitude of stress on the growing rods [48]. But, the focus of this study is the trend and spatial distribution of stress more than the amplitude.

Overall, this finite element modeling approach enables simulation of traditional growing rod fractures based on the clinical patient registry data. After sufficient verification, validation, and uncertainty quantification, this method may supplement the experimental techniques for characterizing traditional growing rod failures. The evidence from this study may encourage device manufactures to implement optimization of growing rods to spatial stress distribution in long constructs to predict growing rod failure. Furthermore, this study also provides information to the surgeons/users about the high stress regions, so that they are aware of these regions and may take special care during surgical implantation.

#### Conclusions

The result of this proof-of-concept study confirms that the rod fracture locations on traditional growing rods, as identified in the retrieval analysis performed by FDA, were indeed high stress regions. The results

further validate the patient-specific approach adopted for FEA modeling in this study. This study shows potential in understanding implant failure from a biomechanical perspective that can be vital for surgical planning and implant design for future cases. The study also highlights the potential of utilizing retrospective clinical/patient registry data to improve on the incumbent state of spinal treatment; providing a detailed biomechanical analysis on traditional growing rod failure which remains a problem in the treatment of early-onset scoliosis.

#### **Declarations of Competing Interests**

Dr. Aakash Agarwal reports Director of Research position at Spinal Balance, and editorial board position from Clinical Spine Surgery, Spine, outside the submitted work (thus doesn't influence the work reported in this paper).

#### Acknowledgements & Funding disclosure

We would like to thank the entire Growing Spine Foundation for their collaboration with the US FDA via a Research Collaborative Agreement in order to use the registry data for this study. We would like to acknowledge the NSF-IUCRC center (CDMI) at the University of Toledo and the University of California-San Francisco for supporting this study in part. We would also like to thank resident spine surgeon Justin Lemans for helping us with the Surgimap software and measurements.

#### Supplementary materials

Supplementary material associated with this article can be found, in the online version, at doi:10.1016/j.xnsj.2020.100043.

#### References

- [1] Ahmad AA, Agarwal A. Active apex correction: an overview of the modified SHILLA technique and its clinical efficacy. J Clin Orthopaed Trauma Sep 1, 2020;11(5):848–52.
- [2] Akbarnia BA, Breakwell LM, Marks DS, McCarthy RE, Thompson AG, Canale SK, Kostial PN, Tambe A, Asher MAGrowing Spine Study Group. Dual growing rod technique followed for three to eleven years until final fusion: the effect of frequency of lengthening. Spine Apr 20, 2008;33(9):984–90.
- [3] Thompson GH, Akbarnia BA, Kostial P, Poe-Kochert C, Armstrong DG, Rog J, Lowe R, Asher MA, Marks DS. Comparison of single and dual growing rod techniques followed through definite surgery: a preliminary study. Spine (Phila Pa 1976) 2005;30(18):2039-44.
- [4] Agarwal A, Kelkar A, Agarwal AG, Jayaswal D, Jayaswal A, Shendge V. Device-related complications associated with MAGEC rod usage for distraction-based correction of scoliosis. Spine Surg Relat Res 2020;4(2):148–51.
- [5] Agarwal A, Aker L, Ahmad AA. Active apex correction with guided growth technique for controlling spinal deformity in growing children: a modified SHILLA technique. Global Spine J. Jun 2020;10(4):438–42.
- [6] Lemans J, Kodigudla M, Kelkar A, Kruyt M, Goel V, Agarwal A. Spring distraction system for early onset scoliosis provides continuous distraction without a potential increase in rod fractures, compared to traditional growing rods. Spine Deform Nov 1, 2018;6(6):819–20.
- [7] McCarthy Richard E, McCullough Frances L. Shilla growth guidance for early-onset scoliosis: results after a minimum of five years of follow-up. JBJS 2015;97(19):1578–84.
- [8] Agarwal A, Aker L, Ahmad AA. Active apex correction (Modified SHILLA Technique) versus distraction-based growth rod fixation: what do the correction parameters say? Spine Surg Relat Res 2020;4(1):31–6.

- [9] Sankar WN, Acevedo DC, Skaggs DL. Comparison of complications among growing spinal implants. Spine 2010;35(23):2091-6.
- [10] Greggi T, Lolli F, Di Silvestre M, Martikos K, Vommaro F, Maredi E, Giacomini S, Baioni A, Cioni A. Complications incidence in the treatment of early onset scoliosis with growing spinal implants. Stud Health Technol Inform Jun 19. 2012;176:334–7.
- [11] Shinohara K, Takigawa T, Tanaka M, Sugimoto Y, Arataki S, Yamane K, Watanabe N, Ozaki T, Sarai T. Implant failure of titanium versus cobalt-chromium growing rods in early-onset scoliosis. Spine Mar 15, 2016;41(6):502–7.
- [12] Bess S, Akbarnia BA, Thompson GH, Sponseller PD, Shah SA, El Sebaie H, Boachie-Adjei O, Karlin LI, Canale S, Poe-Kochert C, Skaggs DL. Complications of growing-rod treatment for early-onset scoliosis: analysis of one hundred and forty patients. JBJS Nov 3. 2010;92(15):2533–43.
- [13] Beaven A, Gardner AC, Marks DS, Mehta JS, Newton-Ede M, Splisbury JB. Magnetically controlled growing rods: the experience of mechanical failure from a single center consecutive series of 28 children with a minimum follow-up of 2 Years. Asian Spine J 2018;12(5):794–802.
- [14] Lebon J, Batailler C, Wargny M, Choufani E, Violas P, Fron D, Kieffer J, Accadbled F, Cunin V, De Gauzy JS. Magnetically controlled growing rod in early onset scoliosis: a 30-case multicenter study. Eur Spine J 2017;26(6):1567–76.
- [15] Thakar C, Kieser DC, Mardare M, Haleem S, Fairbank J, Nnadi C. Systematic review of the complications associated with magentically controlled growing rods for the treatment of early onset scoliosis. Eur Spine J 2018;27(9):2062–71.
- [16] Cryar KA, Bumpass DB, McCullough L, McCarthy R. Rod breakage in Shilla growth guidance constructs: when where and why? Spine J 2017;17(10):S107.
- [17] Hill Genevieve, Nagaraja Srinidhi, Akbarnia Behrooz A, Pawelek Jeff, Sponseller Paul, Sturm Peter, Emans John, et al. Retrieval and clinical analysis of distraction-based dual growing rod constructs for early-onset scoliosis. Spine J 2017;17(10):1506–18.
- [18] Prendergast PJ. Finite element models in tissue mechanics and orthopaedic implant design. Clin Biomech 1997;12(6):343–66.
- [19] Harrysson Ola LA, Hosni Yasser A, Nayfeh Jamal F. Custom-designed orthopedic implants evaluated using finite element analysis of patient-specific computed tomography data: femoral-component case study. BMC Musculoskel Disord 2007;8(1):91.
- [20] Schuller HM, et al. Total hip reconstruction in acetabular dysplasia. A finite element study. J Bone Joint Surg Br 1993;75(3):468–74.
- [21] Agarwal A, Palepu V, Agarwal AK, Goel VK, Yildirim ED. Biomechanical evaluation of an endplate-conformed polycaprolactone-hydroxyapatite intervertebral fusion graft and its comparison with a typical nonconformed cortical graft. J Biomech Eng Jun 1, 2013;135(6).
- [22] Kiapour A, Palepu V, Kiapour A, Demetropoulos C. Finite element analysis. In: Dynamic reconstruction of the spine, 10. Thieme; 2015. p. 75–84.
- [23] Matsuura Y, Giambini H, Ogawa Y, Fang Z, Thoreson AR, Yaszemski MJ, Lu L, An KN. Specimen-specific nonlinear finite element modeling to predict vertebrae fracture loads after vertebroplasty. Spine Oct 15, 2014;39(22):E1291.
- [24] van Rijsbergen M, van Rietbergen B, Barthelemy V, Eltes P, Lazáry Á, Lacroix D, Noailly J, Tho MC, Wilson W, Ito K. Comparison of patient-specific computational models vs. clinical follow-up, for adjacent segment disc degeneration and bone remodelling after spinal fusion. PloS One Aug 30, 2018;13(8):e0200899.
- [25] Gefen A, editor. Patient-specific modeling in tomorrow's medicine. Springer; Jan 5, 2012.
- [26] Shim V, Gather H, Schreiber G, Peldschus A, Josten B. Development of a patient-specific finite element model for predicting implant failure in pelvic ring fracture fixation. Comput Math Methods Med 2017.
- [27] Miles B, Kolos E, Walter WL, Appleyard R, Shi A, Li Q, Ruys AJ. Subject specific finite element modeling of periprosthetic femoral fractures using element deviation to simulate bone failure. Med Eng Phys 2015;37(6):567–73.
- [28] Esposito L, Bifulco P, Gargiulo P, Gislason MK, Cesarelli M, Iuappariello L, Jonsson H, Cutolo A, Fraidi M. Towards a patient-specific estimation of intra-operative femoral fracture risk. Comput Methods Biomech Biomed Eng 2018;27:1–10.
- [29] Pettersen SH, Wik TS, Skallerud B. Subject specific finite element analysis of implant stability for a cementless femoral stem. Clin Biomech (Bristol, Avon) 2009;24(6):480–7.

- [30] Al-Dirini RMA, Huff D, Zhang J, Besier T, Clement JG, Taylor M. Influence of collars on the primary stability of cementless femoral stems: a finite element study using a diverse patient cohort. J Orthoped Res 2018;36(4):1185–95.
- [31] Helgason B, Palsson H, Runarsson TP, Frossard L, Viceconti M. Risk of failure during gait for direct skeletal attachment of a femoral prosthesis: a finite element study. Med Eng Phys 2009;31(5):595–600.
- [32] Albogha MH, Kitahara T, Todo M, Hyakutake H, Takahashi I. Maximum principal strain as a criterion for prediction of orthodontic mini-implants failure in subject specific finite element models. Angle Orthod 2016;86(1):24–31.
- [33] Le Navéaux F, Larson AN, Labelle H, Wang X, Aubin CÉ. How does implant distribution affect 3D correction and bone-screw forces in thoracic adolescent idiopathic scoliosis spinal instrumentation? Clin Biomech Nov 1, 2016;39:25–31.
- [34] Wang X, Boyer L, Le Naveaux F, Schwend RM, Aubin CE. How does differential rod contouring contribute to 3-dimensional correction and affect the bone-screw forces in adolescent idiopathic scoliosis instrumentation? Clin Biomech Nov 1, 2016;39:115–21.
- [35] Wang X, Larson AN, Crandall DG, Parent S, Labelle H, Ledonio CG, Aubin CE. Biomechanical effect of pedicle screw distribution in AIS instrumentation using a segmental translation technique: computer modeling and simulation. Scol Spinal Disord Dec, 2017;12(1):13.
- [36] Agarwal Aakash, Jayaswal Arvind, Goel Vijay K, Agarwal Anand K. Patient-specific distraction regimen to avoid growth-rod failure. Spine 2018;43(4):E221–6.
- [37] Agarwal Aakash, Agarwal Anand K, Jayaswal Arvind, Goel Vijay. Smaller interval distractions may reduce chances of growth rod breakage without impeding desired spinal growth: a finite element study. Spine Deform 2014;2(6):430-6.
- [38] Agarwal Aakash, Agarwal Anand K, Jayaswal Arvind, Goel Vijay K. Outcomes of optimal distraction forces and frequencies in growth rod surgery for different types of scoliotic curves: an in silico and in vitro study. Spine Deform 2017;5(1):18–26.
- [39] Agarwal Aakash, Zakeri Amanda, Agarwal Anand K, Jayaswal Arvind, Goel Vijay K. Distraction magnitude and frequency affect the outcome in juvenile idiopathic patients with growth rods: finite element study using a representative scoliotic spine model. Spine J 2015;15(8):1848–55.
- [40] Agarwal Aakash, Agarwal Anand K, Jayaswal Arvind, Goel Vijay K. Effect of distraction force on growth and biomechanics of the spine: a finite element study on normal juvenile spine with dual growth rod instrumentation. Spine Deform 2014;2(4):260–9.
- [41] Lenke LG. Lenke classification system of adolescent idiopathic scoliosis: treatment recommendations. Instruct Course Lect 2005;54:537–42.
- [42] Ovadia D. Classification of adolescent idiopathic scoliosis (AIS). J Child Orthopaed Feb 1, 2013;7(1):25–8.
- [43] Agarwal Aakash. Mitigating biomechanical complications of growth rods in juvenile idiopathic scoliosis; 2015. p. 1824.
- [44] Tauchi R, et al. Reliability analysis of Cobb angle measurements of congenital scoliosis using X-ray and 3D-CT images. Eur J Orthop Surg Traumatol 2016;26(1):53–7.
- [45] Tanure MC, Pinheiro AP, Oliveira AS. Reliability assessment of Cobb angle measurements using manual and digital methods. Spine J 2010;10(9):769–74.
- [46] Schultz A, Andersson GB, Ortengren R, Bjork R, Nordin M. Analysis and quantitative measurements of loads on the lumbar spine when holding weights in standing posture. Spine (Phila Pa 1976) 1982;7(4):390–7.
- [47] Agarwal Aakash, Goswami Ankur, Vijayaraghavan Govindaraja Perumal, Srivastava Abhishek, Kandwal Pankaj, Nagaraja Upendra Bidre, Goel Vijay K, Agarwal Anand K, Jayaswal Arvind. Quantitative characteristics of consecutive lengthening episodes in early onset scoliosis (EOS) patients with dual growth rods. Spine 2018.
- [48] Schlager B, Niemeyer F, Galbusera F, Volkheimer D, Jonas R, Wilke JH. Uncertainty analysis of material properties and morphology parameters in numerical models regarding the motion of lumbar vertebral segments. Comput Methods Biomech Biomed Eng 2018;21(12):673–83.